Journal of Materials Chemistry A

Accepted Manuscript

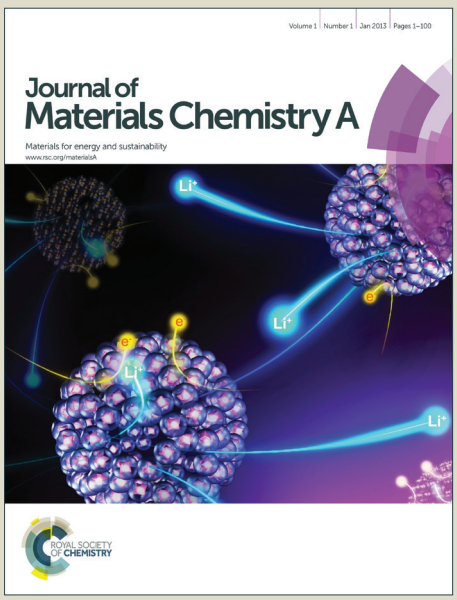

ROYAL SOCIETY OF CHEMISTRY

www.rsc.org/materialsA

Journal Name

RSCPublishing

ARTICLE

Cite this: DOI: 10.1039/xoxxoooooox

Received ooth January 2012,
Accepted ooth January 2012

DOI: 10.1039/xoxxoooooox

www.rsc.org/

Dimensionally Integrated Nanoarchitectonics for Novel Composite from 0D, 1D, and 2D Nanomaterials: RGO/CNT/CeO_2 Ternary Nanocomposite with Electrochemical Performance

Raja Rajendran,[a,b] Lok Kumar Shrestha,*[a] Kosuke Minami,[a] Munisamy Subramanian,[b] Ramasamy Jayavel,[b] and Katsuhiko Ariga[a]

We report one-step conversion of dimensionally mixed ternary nanocomposite from zero-dimensional (0D) cerium oxide (CeO_2), one-dimensional (1D) carbon nanotube (CNT), and two-dimensional (2D) reduced graphene oxide (RGO) nanomaterials by chemical precipitation method. The RGO/CNT/CeO_2 ternary nanocomposite showed excellent electrochemical performance (electrical double layer capacitor properties) in aqueous electrolyte followed by long term cyclic stability, and high energy density compared to its binary counterparts.

Introduction

Carbon-based nanostructures such as fullerenes, nanotubes or nanofibers, and graphene have become a common interest of many material scientists, biochemists, and nanotechnologists in the recent years [1-13]. In addition, these nanocarbons exhibit specific properties depending on their dimensions [14-18]. Carbon-based materials can be classified based on dimensionalities of the nanostructures as the entire range of dimensionalities can be found in nanocarbon family such as zero-dimensional (0D) fullerenes or diamond clusters, one-dimensional (1D) nanotubes or nanofibers, two-dimensional (2D) graphene sheet, and three-dimensional (3D) nanocrystalline diamond and fullerite [19,20].

It would be highly expected that integration of these dimensionalities is one of the important keys to develop novel functions in nanocarbon materials. A novel concept, nanoarchitectonics would work on this purpose [21-26].

Carbon nanostructures depending on their dimensions cover wider range of applications including anode materials for rechargeable lithium ion (Li-ion) batteries, optoelectronic devices, biomedicine, sensing, and catalysis. Two-D graphene shows excellent electrical, mechanical, and thermal properties so that it is finding extensive applications in the fields of energy-related materials, sensors, and catalysts [27-29]. Due to its high surface area and good chemical stability, it has also been used as adsorbent, supercapacitor, and support material to design heterogeneous catalysts with enhanced activities. It has been demonstrated that graphene-supported metal or metal oxide nanoparticles enhance hydrogen storage capacity, exhibit high efficiencies for CO oxidation and oxygen reductions, superior electrochemical sensing, and fuel cell applications [30-32].

Design of graphene-based hybrid materials to improve device performance has attracted intense attention and continues to grow. Such novel graphene nanohybrids or nanocomposites can be developed combining graphene with polymers, semiconducting quantum dots, and metallic nanoparticles [33-36]. Graphene/polymer composites have shown enhanced electrical conductivity, electrochemical capacity, and mechanical strength [37]. Similarly, composite of graphene and semiconductor materials have been demonstrated enhanced performance in solar cells, Li-ion batteries and supercapacitors [38,39]. The insertion of novel metallic nanoparticles such as silver and gold into graphene matrix not only result in surface-enhanced Raman scattering (SERS), but also show better catalytic activity and increased sensitivity in electrochemical and chemical sensing. Such materials have also efficiently been used in DNA detection [40-43]. Extensive efforts have been given to incorporate metal nanoparticles on the graphite oxide (GO) sheets and several methods including thermal evaporation, microwave assisted synthesis, photochemical synthesis, and chemical reduction have been developed to attach novel metallic nanoparticles on the GO sheets. However, despite the extensive studies, ternary composites consisting of graphene, carbon nanotubes (CNT), and metal oxides nanocrystals have not been explored yet. Dimensionally mixed multifunctional nanostructures with two or more types of materials using covalent or noncovalent interactions can extend new functionalities in these nanostructures and can open the possibilities of novel applications.

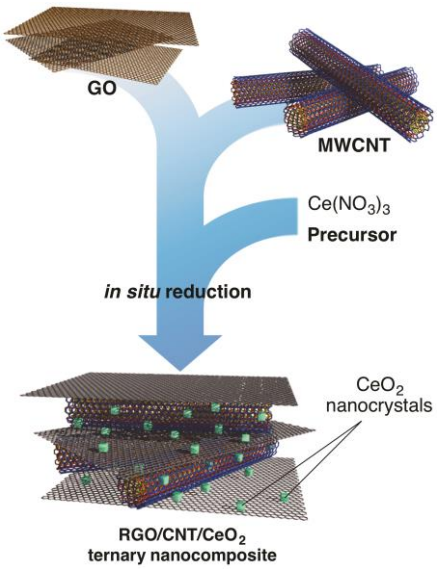

Scheme 1 Schematic representation of dimensionally integrated ternary nanocomposite from 0D CeO_2, 1D CNT, and 2D RGO nanomaterials.

In this contribution, we report the one-step conversion of dimensionally mixed composite from 0D cerium oxide (CeO_2), 1D CNT, and 2D reduced graphite oxide (RGO) nanomaterials into a RGO/CNT/CeO_2 ternary nanocomposite based on materials nanoarchitectonics concept (Scheme 1) and discuss its significant enhancement of electrochemical performance in aqueous electrolyte. This novel composite material is anticipated to offer excellent electrochemical sensing and electrocatalytic activities [44,45]. Although high surface area of RGO is anticipated to exhibit excellent electrochemical properties, due to the inherent limitation of restacking of RGO driven by the π-π interaction suitable spacing material needs to be intercalated into the RGO sheets to avoid the recombination of graphene layers. CNT due to its remarkable thermal, mechanical, and electrical properties derived from their unique structure, high aspect ratio and long range π-π conjugation [46-48] can be a potential candidate as the spacing material to avoid restacking of RGO sheet [49-52]. CNT lying on the basal spacing between the graphene layers avoids RGO stacking and consequently enhances the conductive network for the electron transport within the matrix. Distribution of 0D CeO_2 nanocrystals (an excellent electrochemical redox material) into the RGO/CNT hybrid conducting matrix is found to enhance the electrochemical performance of the ternary composite.

Experimental

Materials

Synthetic graphite powder (average particle size < 20 μm) was purchased from Sigma-Aldrich, Japan. Sulfuric acid, nitric acid, hydrochloric acid and hydrogen peroxide, magnesium nitrate, iron nitrate, ammonium molybdate and citric acid were purchased from Nacalai tesque, Japan. Sodium nitrate, potassium permanganate, and sodium hydroxide were the product of Wako Chemical, Japan. Cerium nitrate was purchased from Sigma-Aldrich Japan. All the materials were used as received without further purifications. De-ionized water was used throughout this study.

Preparation of multi walled carbon nanotube

Multi walled carbon nanotubes (MWCNT) were synthesized by catalytic chemical vapor deposition (CVD) method using Fe-Mo/MgO as a catalyst. For the preparation of catalyst, iron nitrate [$Fe(NO_3)_3.9H_2O$] (0.064 g), ammonium molybdate [$(NH_4)_5Mo_7O_{24}.4H_2O$] (0.061 g), magnesium nitrate [$Mg(NO_3)_2.6H_2O$] (1.153 g) and citric acid [$C_6H_8O_7$] (1.0 g) were dissolved in de-ionized water and stirred for 6 h at 90 °C [53]. The solution was dried at 120 °C for 24 h and calcinated at 550 °C in air for 1 h. The freshly prepared catalyst (100 mg) was placed in a quartz boat inside an alumina tube, nitrogen gas was then passed through the tube at a flow rate of 100 mL/min followed by increasing temperature slowly to 700 °C (at heating rate of 2 °C/min). Once the temperature became 700 °C nitrogen gas supply was stopped and acetylene gas was supplied for 30 min (30 mL/min). Finally, the temperature decreased down to room temperature. The obtained black powder was treated with concentrated HCl to remove impurities, filtered, and dried at 80 °C. The as-prepared carbon nanotubes were functionalized by treating with concentrated HNO_3 at 60 °C for 24 h.

Preparation of graphite oxide (GO)

Graphitic oxide (GO) were synthesized by modified Hummer's method [54]. Graphite powder (2 g) was added to concentrated H_2SO_4 (46 mL) at 0 °C in an ice bath and stirred for 5 min. $NaNO_3$ (1 g) was then added and stirring continued for 5 min. $KMnO_4$ (6g) was added slowly into the resulting mixture and stirring continued for 30 min at 35 °C. H_2O (96 mL) was then added dropwise to the above mixture and temperature was increased to 98 °C and maintained for 30 min then a further aliquot of H_2O (280 mL) was added and stirring was continued for 10 min. Finally, aqueous H_2O_2 (30 mL, 30%) was added dropwise. The initially black colored mixture converted into a reddish-brown color.

Synthesis of RGO/CNT/CeO_2 Composites

The prepared GO (100 mg) was added to water (100 mL) and ultrasonication was applied to the resulting mixture for 2 h in a sonication bath (BRANSON 3510). Functionalized CNT (100 mg) was then added to the GO solution followed by ultrasonication for 1 h. $Ce(NO_3)_3.6H_2O$ (2.17 g) was added to the mixture of GO and CNT solution and stirred for 30 min. NaOH pellet (10 mg) was added to maintain the solution at pH 10. The solution was vigorously stirred for 6 h at 90 °C and filtered followed by repeated washing with de-ionized water and ethanol, and the material was dried at 60 °C under reduced pressure. CNT/CeO_2 and RGO/CeO_2 composites were prepared following the same procedure. CeO_2 nanoparticles were prepared using above conditions without carbon source.

Characterization

The products were characterized by transmission electron microscope (TEM) images. Crystal structures of the samples were

examined by powder X-ray diffraction (XRD). The XRD patterns were measured on an Altima III Rint 2000 (Cu Kα radiation, λ = 1.5418 Å) diffractometer at 25 °C. Fourier transferred-infrared spectroscopy (FT-IR) spectra were recorded using a Nicolet 4700. Raman scattering spectra were recorded on Horiba-Jobin-Yvon T64000 with a 532 nm laser at 25 °C. X-ray photoelectron spectroscopy (XPS) measurements were performed on a Theta Probe spectrometer (Thermo Electron Co. Germany) using monochromated Al–K_α radiation (photon energy 15 KeV, maximum energy resolution ≤ 0.47 eV, and maximum space resolution ≤ 15 μm). High resolution spectra; core level O 1s, Ce 3d, and C1s were recorded in 0.05 eV steps. A built-in electronic charge neutralizing electron flood gun was used to prevent sample charging. Wide spectra in the 1000 – 0 eV binding energy range were recorded. N_2 adsorption isotherms were recorded on Quantachrome Autosorb-iQ2.

Electrochemical performance

The electrochemical properties of the materials were studied using a three-electrode system in 1M Na_2SO_4 aqueous solution at room temperature (25 °C). A bare glassy carbon electrode (GCE) as working electrode was mirror polished with Al_2O_3 slurry and rinsed with double-distilled water and sonicated in acetone for 5 min. The working electrode was modified by dispersing RGO/CNT/CeO_2 ternary composites (10 mg) in methanol solution (1 mL) to form slurry. The slurry was sonicated for 10 min and 10 μL of the slurry was placed on the GCE surface and dried at room temperature for 3 h. Five μL of Nafion solution (0.25%) was added on the modified working electrode surface as binder and dried at 70 °C for 1 h. Working electrodes for CeO_2, and CNT/CeO_2 were prepared using the same method. Platinum wire was used as a counter electrode and a Ag/AgCl as the reference electrode. The cyclic voltammetry (CV) and chronopotentiometry at –1 to 0 V were performed on a CH instruments model: (CHI 850D Work station (USA)). The specific capacitance (C_s) was calculated from the discharge curves using equation (1) [55,56].

$$C_s = \frac{It}{\Delta V \times m} \qquad (1)$$

Where, C_s, I, t, ΔV, and m are the specific capacitance (F g^{-1}), discharge current (A), the discharge time (s), potential window, and mass of the active material, respectively.

Results and discussion

Dimensionally mixed ternary nanocomposite (RGO/CNT/CeO_2) containing 0D CeO_2 nanoparticles distributed on 1D CNT and 2D RGO nanomaterials was prepared in a single step by chemical precipitation method with in situ reduction. An ultrasonication was applied to the aqueous mixture of GO and MWCNT and $Ce(NO_3)_3$, precursor of cerium nanoparticle followed by a vigorous stirring at 90 °C under basic condition (pH = 10) to obtain the precipitate of the RGO/CNT/CeO_2 ternary nanocomposite. CNT/CeO_2 binary nanocomposite was also prepared using the same procedure. Fig. 1 shows TEM images of CNT/CeO_2 and RGO/CNT/CeO_2. CNT/CeO_2 binary nanocomposite clearly showed that CeO_2 nanocubes were formed with the average size of 10 nm, were attached on the surface of CNT, and well distributed to the CNT network (Fig. 1a and b).

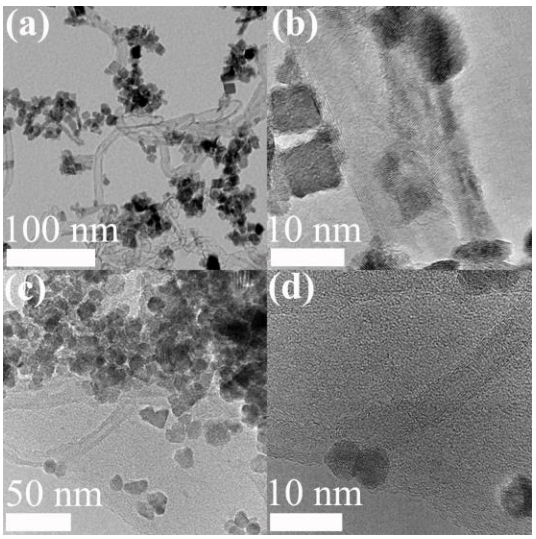

Fig. 1 TEM (a) and HRTEM (b) images of CNT/CeO_2, and TEM (c) and HRTEM (d) image of RGO/CNT/CeO_2 ternary nanocomposite.

Additional TEM images of CNT/CeO_2 binary composite are supplied in Fig.S1 of the Electronic Supporting Information (ESI). In the RGO/CNT/CeO_2 ternary nanocomposite, 0D CeO_2 nanoparticles were uniformly distributed on the surface of CNT and RGO sheet (Fig. 1c and d). Additional TEM (Fig.S2) and HR-TEM images (Fig.S3) of RGO/CNT/CeO_2 ternary composite are supplied in ESI. Fig.S4 shows results of TEM/EDS elemental mapping.

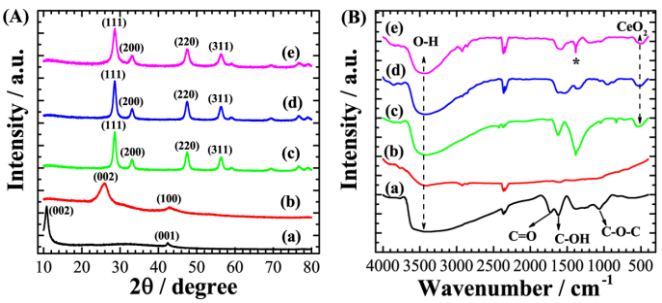

Fig. 2 (A) XRD patterns of GO (a), CNT (b), CeO_2 (c), CNT/CeO_2 (d), and RGO/CNT/CeO_2 ternary nanocomposite (e), (B) FTIR spectra of GO (a), CNT (b), CeO_2 (c), CNT/CeO_2 (d), and RGO/CNT/CeO_2 (e). In panel (B) * represents skeletal vibration of graphene sheets.

The crystal phase and structure information of the RGO/CNT/CeO_2 ternary nanocomposite was identified by XRD measurement (Fig. 2A). The XRD patterns of CNT/CeO_2 binary and RGO/CNT/CeO_2 ternary nanocomposites showed four major peaks at 28.5°, 33.1°, 47.5°, and 56.3°, which correspond respectively to (111), (200), (220), and (311) planes of face-center cubic CeO_2 (JCPDS 78–0694). Using Debye-Scherrer's equation, average crystalline sizes of cerium nanocrystals in CNT/CeO_2 and RGO/CNT/CeO_2 were 12 ± 0.5 and 11 ± 0.5 nm, respectively. Diffraction peaks of GO and MWCNT

were not observed in the RGO/CNT/CeO_2 ternary nanocomposite due to low degree of graphitization caused by the deposition of CeO_2 nanoparticles on their surfaces [57].

To reveal the surface functional groups and the interaction among the three components in the RGO/CNT/CeO_2 ternary nanocomposite, FTIR measurements were conducted (Fig. 2B). For the CNT/CeO_2 binary nanocomposite, the characteristic peaks of functionalized CNT at 2925 (C–H asymmetric stretching), 2854 (C–H symmetric stretching), 3410 (O–H stretching), 1603 (C=O stretching), 1420 (C=C stretching), 1265 (O–H bending vibration) and 1080 cm^{-1} (C–O stretching vibration) were observed with the observation of the Ce–O stretching peak at 511 cm^{-1} [58]. This result also supports the formation of CeO_2 nanoparticles on the surface of CNT (Fig 2B(c), (d) and (e)). In the RGO/CNT/CeO_2 ternary nanocomposite, skeletal vibration of C=C (1558 cm^{-1} as by * in Fig. 2B(e)) and C–O–C stretching (1054 cm^{-1}) of GO, and Ce–O stretching (490 cm^{-1}) were clearly observed in comparison with GO and CNT/CeO_2 though the carbonyl (1724 cm^{-1}) disappeared (Fig. 2B(e)) [59]. These results not only indicate the formation of CeO_2 nanoparticles but also confirm the conversion of GO into RGO during the preparation of RGO/CNT/CeO_2 ternary nanocomposite by in situ reduction [60].

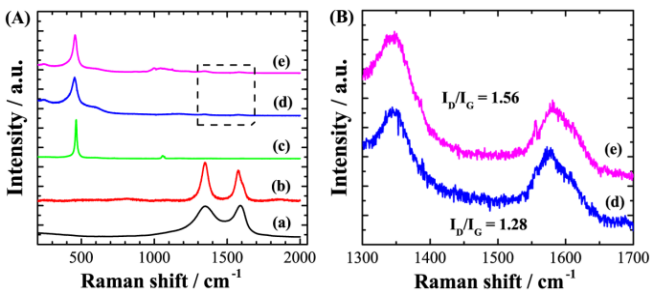

Fig. 3 (A) Raman scattering spectra of CNT (a), GO (b), CeO_2 (c), CNT/CeO_2 (d) and RGO/CNT/CeO_2 ternary nanocomposite (e), (B) Raman spectra highlighting D and G band of CNT/CeO_2 (d), and RGO/CNT/CeO_2 ternary composite (e).

Further characterization of RGO/CNT/CeO_2 ternary nanocomposite was performed by Raman spectroscopy, which is known a non-destructive method to characterize carbon-based materials. Raman spectra of GO, CNT, CeO_2, CNT/CeO_2, and RGO/CNT/CeO_2 are shown in Fig. 3. A strong Raman band appeared at 463 cm^{-1} for CeO_2 nanocrystal (Fig. 3A(c)) can be assigned to the triply degenerate F_{2g} mode as a symmetrical stretching mode of the Ce–O8 vibration unit. The F_{2g} vibrational mode is sensitive to the disorder in oxygen sublattice, which usually occurs during oxygen doping and also the thermally induced non-stoichiometry effect [61]. A blue shift (band shifted from 463 to 453 cm^{-1}) corresponding to the F_{2g} mode is observed in the Raman spectrum of the CNT/CeO_2 (Fig. 3A(d)). A similar blue shift (from 463 to 455 cm^{-1}) is observed in the RGO/CNT/CeO_2 system (Fig. 3A(e)). These blue shifts are the clear evidences of the charge transfer between CeO_2 and CNT, and CeO_2 and RGO [62].

In order to estimate the disorder structure of RGO and CNT in prepared composite materials, we have displayed the intensity ratio of D band to G band (I_D/I_G) in Fig. 3B. Clear D (1353 cm^{-1}) and G bands (1592 cm^{-1}) are observed in CNT, GO, CNT/CeO_2 and RGO/CNT/CeO_2 (Fig. 3A(a), (b) and Fig. 3B(d), (e)). From intensity ratio of D and G bands (I_D/I_G), CNT/CeO_2 binary (1.28) and RGO/CNT/CeO_2 ternary composites (1.56) (Fig. 3B) were more disordered structures than functionalized CNT (I_D/I_G 1.12). This observation is consistent with the corrugation and scrolling structure observed by transmission electron microscopy (TEM). Moreover, the I_D/I_G ratio of RGO/CNT/CeO_2 was higher compared with those of CNT/CeO_2 and GO (I_D/I_G 0.93), which can be attributed to the reduction of oxygen-containing functional groups (i.e. conversion GO into RGO, as I_D/I_G for RGO is calculated 1.2 [63]). This indicates the restoration of the graphene sheets. Minute observations of Raman spectra revealed that the D and G bands of the CNT/CeO_2 and RGO/CNT/CeO_2 composites slightly shifted towards higher frequency, which could be due to different C–C bond length of CNT and C–CeO_2 [63].

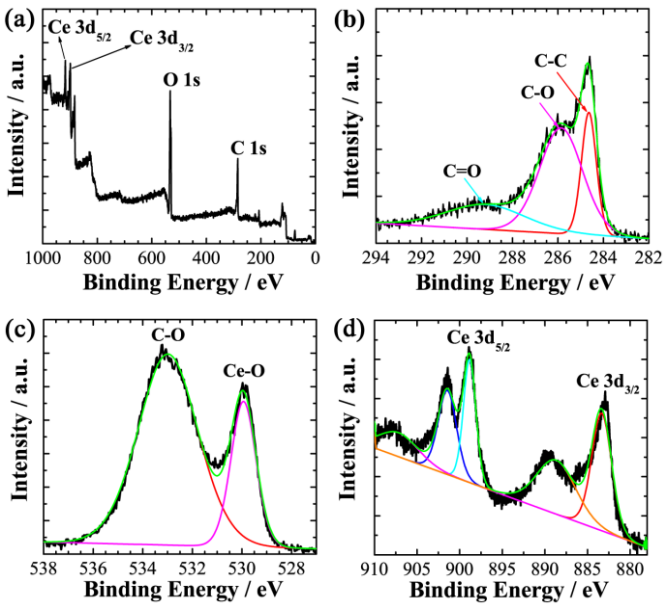

Fig. 4 XPS survey spectra of RGO/CNT/CeO_2 ternary composites (a), C 1s deconvoluted spectra (b), O 1s deconvoluted spectra (c), and Ce 3d deconvoluted spectra (d).

Chemical state of elements in the ternary RGO/CNT/CeO_2 nanocomposite and the extent of reduction of GO to RGO has confirmed by X-rays photoelectron spectroscopy (XPS). A survey XPS spectrum of RGO/CNT/CeO_2 presented in Fig. 4(a) clearly shows the presence of C 1s, O ls, and Ce 3d elements in the RGO/CNT/CeO_2 nanocomposite. As shown in Fig. 4(b), XPS C 1s peak can be deconvoluted into three peaks at 284.7, 286.0, and 289.1 eV. The binding energy of 284.7 eV is a typical peak position for graphitic carbon and demonstrates sp^2-hybridized carbon in the graphene state. The peaks at 286.0, and 289.1 eV can be attributed to the C–O, and C=O oxygen containing carbonaceous bands [64,65]. XPS spectrum of O 1s in Fig. 4(c) can also be deconvoluted into two peaks with peak maximum at 529.8 eV for the Ce–O, and 533.0 eV for the C–O, respectively. Previous studies showed that XPS O 1s spectrum of GO contains carboxylate (C–OH) and carbonyl group

(C=O), the peak at ~533 eV and ~528 eV corresponding to oxygen functional group [63]. These results suggest that the GO converted into RGO by in-situ reduction due to binding of cerium precursor and oxygen functional groups. In Fig 4(d) we have presented XPS spectrum of cerium 3d. The 3d cerium XPS spectrum could be deconvoluted into five peaks; 883.53, 888.91, 899.02, 901.53, and 907.62 eV. The peaks with binding energy 883.53 and 899.02 eV corresponds to the Ce^{3+} ions, whereas, the peaks observed at 888.91, 901.53, and 907.62 eV correspond to Ce^{4+} ions [63]. The CeO_2 has a fluorite crystal structure, and Ce^{4+} cation is surrounded by $8O^{2-}$ anions and O^2 are organized with Ce^{4+}. Presence of Ce^{3+} ions introduces oxygen vacancies in crystal, such high oxygen vacancies show charge transfer effect from the CeO_2 to CNTs/RGO [63].

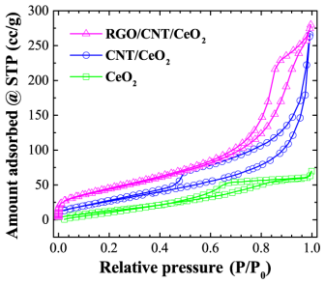

Fig. 5 Nitrogen adsorption/desorption isotherms of CeO_2, CNT/CeO_2, and RGO/CNT/CeO_2 composites.

To avoid restacking of graphene sheets and irreversible agglomeration due to van der Waals interactions during electrode preparation, CNT could introduce as spacers into the graphene layers. Improving the electrochemical performance of the composites, surface areas of the prepared materials were evaluated by nitrogen adsorption/desorption isotherms (Fig. 5). All the isotherms exhibit type IV adsorption isotherm with the H1 hysteresis loop. According to the isotherms, the surface area was calculated by using Brunauer–Emmett–Teller (BET) method. The surface area of CeO_2 nanoparticles and CNT/CeO_2 binary nanocomposite were 60.8 $m^2\ g^{-1}$ and 110.8 $m^2\ g^{-1}$ with the pore volume of 0.11 $cm^3\ g^{-1}$ and 0.28 $cm^3\ g^{-1}$, respectively. After the formation of the RGO/CNT/CeO_2 ternary nanocomposite, the surface area significantly increased to 160 $m^2\ g^{-1}$, and the corresponding pore volume increased to 0.42 $cm^3\ g^{-1}$. It is anticipated that introduction of RGO in the composite reduces the aggregation of CeO_2 that leads to high surface area.

In order to access the surface area offered by our material, we have studied the electrochemical performance of ternary nanocomposite in aqueous electrolyte. Fig. 6 shows cyclic voltammetry (CV) curves of CNT/CeO_2 and RGO/CNT/CeO_2 nanocomposite within the potential range from –1.0 to 0.0 V measured at different scan rates (5–100 mV/s). The CV curves of CeO_2 nanoparticles are shows in Fig.S5. The CV curves of CNT/CeO_2 (Fig. 6a) show rectangular shape at all scan rates showing the electrical double layer capacitor behaviour. The absence of redox peak of CeO_2 is believed to be due to synergistic of CeO_2 with the double layer capacitance of CNT network. Charging and discharging occurs at pseudo constant rate during entire volumetric cycle. Note that CeO_2 itself gives small capacitance. The capacitance of CeO_2 can be improved by mixing with CNT though enhancement is not so high. Significant enhancement in the electrochemical performance could be achieved in the RGO/CNT/CeO_2 ternary nanocomposite (Fig. 6b). The overall window size of the CV curve of RGO/CNT/CeO_2 has drastically expanded which is an indication of the enhanced capacitance compare to the CNT/CeO_2. The excellent capacitive properties of ternary composite can be attributed to homogenous distribution of CeO_2 nanoparticle on to CNT and high electrical conductivity of the RGO.

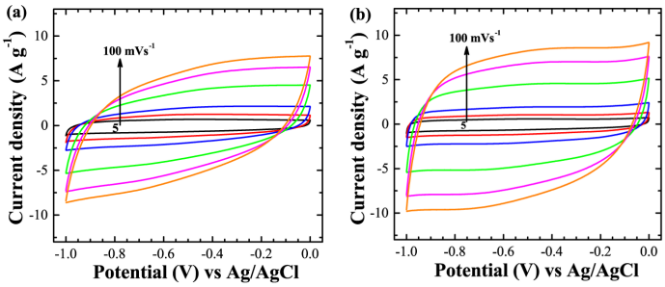

Fig. 6 Electrochemical performances of CNT/CeO_2 binary and RGO/CNT/CeO_2 ternary composite: CV curves of CNT/CeO_2 (a), and corresponding CV curves of RGO/CNT/CeO_2 composites (b) at different scan rates of 5, 10 20, 50, 80, 100 mVs^{-1} in 1M Na_2SO_4 solution.

Galvanostatic charge–discharge (C-D) curves of CeO_2, CNT/CeO_2 and RGO/CNT/CeO_2 electrodes prepared on the glassy carbon support were recorded at different current densities in the potential range of –1.0 to 0 V (Fig. 7).

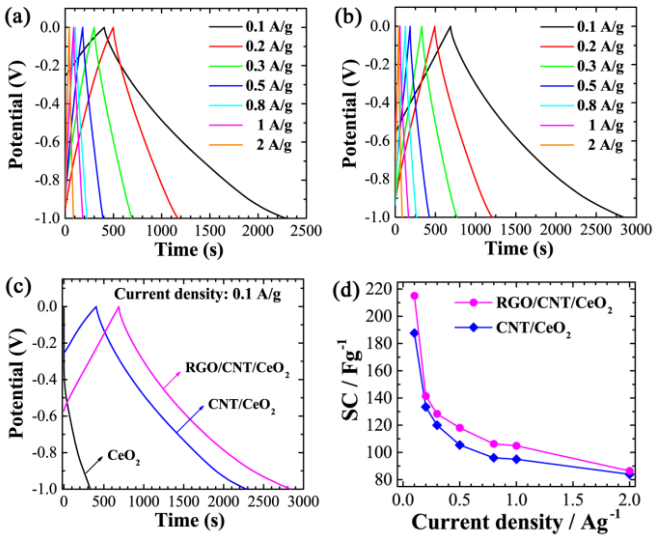

Fig. 7 Chronopotentiometry (charge/discharge curve) of CNT/CeO_2 electrode at different current densities (a), charge/discharge curves of RGO/CNT/CeO_2 electrode at different current densities (b), charge/discharge curve of all electrodes at a constant current density of 0.1 A g^{-1} (c), and calculated specific capacitance of CNT/CeO_2 and RGO/CNT/CeO_2 composites at different current densities (d).

Fig. 7(a) and (b) compares the C-D curves of CNT/CeO_2 and RGO/CNT/CeO_2 at different current densities (0.1 to 2.0 A g^{-1}). A rapid response of the electrodes is observed in both the system; the response of electrode increases with increasing the current density. Fig. 7c shows the electrochemical response of CeO_2, CNT/CeO_2 and RGO/CNT/CeO_2 electrodes at 0.1 A g^{-1}. The RGO/CNT/CeO_2 electrode clearly shows longer discharge time compared to CeO_2 and CNT/CeO_2 electrodes. The extended discharge time is attributed to the combination of RGO, CNT and CeO_2, which offers a larger charge capacity in consistent with the CV profiles. Fig. 7d shows the calculated specific capacitance versus current density for CeO_2 nanoparticle, CNT/CeO_2 binary composite, and RGO/CNT/CeO_2 ternary nanocomposite. At current density of 0.1 A g^{-1}, the specific capacitance of CeO_2, CNT/CeO_2, and RGO/CNT/CeO_2 is ca. 37, 188, and 215 F g^{-1}, respectively. This demonstrates that the dimensionally mixed composite from 2D RGO, 1D CNT, and 0D CeO_2 nanomaterials: RGO/CNT/CeO_2 ternary nanocomposite is best among individual components or CeO_2 composites with CNT, due to the CNT acting as spacers to preventing the restacking of RGO, and also avoiding the agglomeration of CeO_2 nanoparticles.

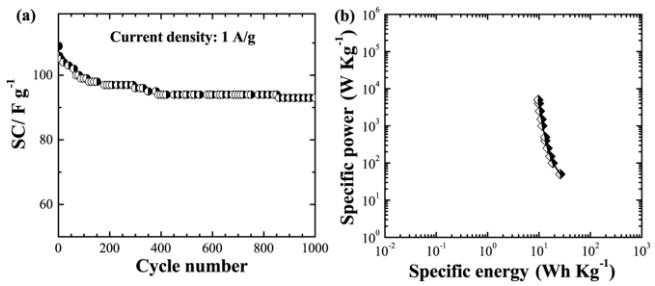

Fig. 8 Cyclic stability (a), and Ragone plot (b) of RGO/CNT/CeO_2 ternary composite.

It is known that the cycle life is important criteria for the supercapacitors. We have carried out the endurance test for CeO_2, CNT/CeO_2 and RGO/CNT/CeO_2 and recorded C-D curves (Fig.S6) for several cycles at 1 A g^{-1}. Fig. 8A shows calculated specific capacitance of RGO/CNT/CeO_2 electrode up to 100 cycles as typical example. Note that the ternary nanocomposite electrode exhibits excellent cycling stability, retaining up to 85% of the initial capacity after 1000 cycles. To further illustrate the energy density and power density are calculated from the charge-discharge curve of RGO/CNT/CeO_2 electrode. The specific energy (SE) and power (SP) were calculated by the using following equations (2) and (3) [66,67]

$$SE = \frac{0.5\ C\ (\Delta V)^2}{3.6} \quad (2)$$

$$SP = SE \times \frac{3600}{t} \quad (3)$$

Where C (F g^{-1}), ΔV and t (s) are a specific capacitance, operating voltage range and discharge time, respectively. Fig. 8b shows the Ragone plot of the voltage window of –1.0 to 0 V at different current densities. The CNT/CeO_2 binary nanocomposite shows the specific energy of 26.05 Wh kg^{-1} at current density of 0.1 A g^{-1}. Compared to CNT/CeO_2, the specific energy of RGO/CNT/CeO_2 electrode showed higher as 29.86 Wh kg^{-1} at 0.1 A g^{-1}, which decreased down to 7.66 Wh kg^{-1} upon increasing current density from 0.1 A g^{-1} to 5 A g^{-1}. Specific power of RGO/CNT/CeO_2 was 49.98 Wkg^{-1} at specific energy of 29.86 Wh kg^{-1}. High specific energy and power were achieved with slow and fast charge-discharge rates, respectively.

The specific power and specific energy offered by the RGO/CNT/CeO_2 ternary nanocomposite is much higher than the conventional capacitors based on CeO_2 nanoparticle/activated carbon (4.86 Wh Kg^{-1}) [68], RGO/CeO_2 (20 Wh Kg^{-1}), CNT/CeO_2 (26.05 Wh Kg^{-1}). These results clearly show the importance of the construction of the dimensionally mixed RGO/CNT/CeO_2 ternary nanocomposite. This novel combination material could be promising supercapacitor materials as RGO and CNT can provide the passage for the electron and charge transport and enhances the electrical conductivity of CeO_2.

Conclusions

We have succeeded to convert 0D (CeO_2), 1D (CNT), and 2D (RGO) nanomaterials into dimensionally mixed RGO/CNT/CeO_2 ternary composite in a single step by chemical precipitation method. Zero-D CeO_2 nanocrystals (with average size of 10 nm) could be homogeneously distributed on the surface of the 2D RGO sheet and 1D CNT, which is functioning as the spacing material to avoid restacking of RGO. The dimensionally mixed composite material RGO/CNT/CeO_2 showed excellent electrochemical performance due to synergistic effects contributed from CNT/RGO and CeO_2 giving specific capacitance value ca. 215 F g^{-1}. The observed high rate capability and 85% of capacity retention after 1000 cycles (long cycle life) demonstrates the importance of dimensionally mixed ternary composite in energy-storage application.

Acknowledgements

RR thanks National Institute for Materials Science (NIMS), Japan and Anna University, India for the NIMS internship award. LKS thanks the Japan Society for the Promotion of Science (JSPS) for the Grants-in-Aid for Young Scientists B (25790021).

Notes and references

[a] International Center for Materials Nanoarchitectonics (WPI-MANA), National Institute for Materials Science (NIMS), 1-1 Namiki, Tsukuba, Ibaraki 305-0044, Japan. Email: SHRESTHA.Lokkumar@nims.go.jp
[b] Centre for Nanoscience and Technology, Anna University, Chennai-600025, India.

Electronic Supplementary Information (ESI) available: [Additional TEM images, CV curve of CeO_2, and elemental mapping]. See DOI: 10.1039/b000000x/

1 W. Nakanishi, K. Minami, L. K. Shrestha, Q. Ji, J. P. Hill and K. Ariga, *Nano Today*, 2014, **9**, 378.
2 Y. Yamada, K. Murota, R. Fujita, J. Kim, A. Watanabe, M. Nakamura, S. Sato, K. Hata, P. Ercius, J. Ciston, C. Y. Song, K. Kim, W. Regan, W. Gannett and A. Zett, *J. Am. Chem. Soc.*, 2014, **136**, 2232.

3 M. Yankowitz, J. I-Jan Wang, A. G. Birdwell, Y.-A, Chen, K. Watanabe, T. Taniguchi, P. Jacquod, P. J. Y. Kim and S. O. Kim, *Nat. Mater.*, 2014, **13**, 325.
4 J. Kim, Y. Yamada and S. Sato, *J. Phys. Chem. C*, 2014, **118**, 7085.
5 P. Yu. X. Wen, Y. R. Toh, Y. C. Lee, K. Y. Huang, S. Huang, S. Shrestha, G. Conibeer and J. Tang. *J. Mater. Chem. C*, 2014, **2**, 2894.
6 M. Li, S. Ishihara, K. Ohkubo, M. Liao, Q. Ji, C. Gu, Y. Pan, X. Jiang, M. Akada, J. P. Hill, T. Nakanishi, Y. Ma, Y. Yamauchi, S. Fukuzumi and Katsuhiko Ariga. *Small*, 2013, **9**, 2064.
7 L. K. Shrestha, Y. Yamauchi, J. P. Hill, K. Miyazawa and K. Ariga, *J. Am. Chem. Soc.*, 2013, **135**, 586.
8 J. Kim, C. Park, J. E. Park, K. Chu and H. C. Choi, *ACS Nano*, 2013, **7**, 9122.
9 X. Zhang, S. Mizukami, T. Kubota, Q. Ma, M. Oogane, H. Naganuma, Y. Ando and T. Miyazaki, *Nat. Commun.*, 2013, **4**, 1392.
10 Q. Ji, I. Honma, S.-M. Paek, M. Akada, J. P. Hill, A. Vinu and K. Ariga. *Angew. Chem. Int. Ed.*, 2010, **49**, 9737.
11 Y. Miyauchi, *J. Mater. Chem. C*, 2013, **1**, 6499.
12 G. Zhang, R. Zhou and X. C. Zeng, *J. Mater. Chem. C*, 2013, **1**, 4518.
13 S. Kopyl, V. Bystrov, I. Bdikin, M. Maiorov and A. C. M. Sousa, *J. Mater. Chem. C*, 2013, **1**, 2860.
14 M. Russ, S. S. Rahatekar, K. Koziol, B. Farmer and H.X Peng, *Composite Sci. Technol.* 2013, **81**, 42.
15 L. K. Shrestha, J. P. Hill, T. Tsuruoka, K. Miyazawa and K. Ariga, *Langmuir*, 2013, **29**, 684.
16 B. W. Jeong and H. Y. Kim, *Phys. Status Solidi A*, 2013, **210**, 1832.
17 A. Cao and J. Qu, *J. Appl. Phys.* 2012, **112**, 013503.
18 A. S. Barnard and I. K. Snook, *J. Mater. Chem.*, 2010, **20**, 10459.
19 M. Inagaki, *New carbons*, Elsevier, 2000.
20 C. N. R. Rao, K. Biswas, K. S. Subrahmanyam and A. Govindaraj, *J. Mater. Chem.*, 2009, **19**, 2457.
21 K. Ariga, Y. Yamauchi, Q. Ji, Y. Yonamine and J. P. Hill, *APL Mater.*, 2014, **2**, 030701.
22 M. Ramanathan, L. K. Shrestha, T. Mori, Q. Ji, J. P. Hill and K. Ariga, *Phys. Chem. Chem. Phys.* 2013, **15**, 10580.
23 K. Ariga, Q. Ji, T. Mori, M. Naito, Y. Yamauchi, H. Abe and J. P. Hill. *Chem. Soc. Rev.*, 2013, **42**, 6322.
24 L. K. Shrestha, Q. Ji, T. Mori, K. Miyazawa, Y. Yamauchi, J. P. Hill and K. Ariga, *Chem. Asian J.*, 2013, **8**, 1662.
25 L. K. Shrestha, R. G. Shrestha, J. P. Hill and K. Ariga, *J. Oleo Sci.*, 2013, **62**, 541.
26 K. Ariga, T. Mori and J. P. Hill, *Langmuir*, 2013, **29**, 8459.
27 Y. Zhu, S. Murali, W. Cai, X. Li, J. W. Suk, J. R. Potts and R. S. Ruoff, *Adv. Mater.*, 2010, **22**, 3906.
28 Y. Gao, D. Ma, C. Wang, J. Guan and X. Bao, *Chem. Commun.*, 2011, **47**, 2432.
29 Z. Jin, D. Nackashi, W. Lu, C. Kittrell and J. M. Tour, *Chem. Mater.*, 2010, **22**, 5695.
30 H. Bai, C. Li and G. Shi, *Adv. Mater.*, 2011, **23**, 1089.
31 S. Zhang, Y. Shao, H. Liao, J. Liu, I.A. Aksay, G. Yin and Y. Lin, *Chem. Mater.*, 2011, **23**, 1079.
32 J. Huang, L. Zhang, B. Chen, N. Ji, F. Chen, Y. Zhang and Z. Zhang, *Nanoscale*, 2010, **2**, 2733.
33 O. C. Compton and S. T. Nguyen, *Small*, 2010, **6**, 711.
34 K. P. Loh, Q. L. Bao, G. Eda and M. Chhowalla, *Nat. Chem.*, 2010, **2**, 1015.
35 X. Huang, Z. Yin, S. Wu, X. Qi, Q. He, Q. Zhang, Q. Yan, F. Boey and H. Zhang, *Small*, 2011, **7**, 1876.
36 H. Jiang, *Small*, 2011, **7**, 2413.
37 D. D. Kulkarni, I. Choi, S. Singamaneni and V. V. Tsukruk, *ACS Nano*, 2010, **4**, 4667.
38 P. V. Kamat, *J. Phys. Chem. Lett.*, 2010, **1**, 520.
39 S. B. Yang, X. L. Feng, S. Ivanovici and K. Mullen, *Angew. Chem., Int. Ed.*, 2010, **49**, 8408.
40 S. J. Guo, S. J. Dong and E. W. Wang, *ACS Nano*, 2010, **4**, 547.
41 M. Yang, B. G. Choi, T. J. Park, N. S. Heo, W. H. Hong and S.Y. Lee, *Nanoscale*, 2011, **3**, 2950.
42 Y. Du, S. J. Guo, S.J. Dong and E. K. Wang, *Biomaterials*, 2011, **32**, 8584.
43 Y. H. Lee, L. Polavarapu, N. Gao, P. Yuan and Q.-H. Xu, *Langmuir*, 2012, **28**, 321.
44 A. Ambrosi, C. K. Chua, A. Bonanni and M. Pumera, *Chem. Rev.*, 2014, **114**, 7150.
45 M. Pumera, *Electrochem. Commun*, 2013, **36**, 14.
46 Y. Xiao, Q. Zhang, J. Yan, T. Wei, Z. Fan and F. Wei, *J. Electroanal. Chem.*, 2012, **684**, 32.
47 G. Lota, K. Fic and E. Frackowiak, *Energy Environ. Sci.*, 2011, **4**, 1592.
48 Y. T. Kim, K. Tadai and T. Mitani, *J. Mater. Chem.*, 2005, **15**, 4914.
49 R. B. Rakhi and H. N. Alshareef, *J. Power Sources.*, 2011, **196**, 8858.
50 B. Zhang, Q. B. Zheng, Z. D. Huang, S. W. Oh and J. K. Kim, *Carbon*, 2011, **49**, 4524.
51 L. Peng, Y. Feng, P. Lv, D. Lei, Y. Shen, Y. Li and W. Feng, *J. Phys. Chem.C*, 2012, **116**, 4970.
52 Q. Cheng, J. Tang, J. Ma, H. Zhang, N. Shinya and L. C. Qin, *Phys. Chem. Chem. Phys.*, 2011, **13**, 17615.
53 B. C. Liu, S. C. Lyu, S. I. Jung, H. K. Kang, C. W. Yang, J. W. Park, C. Y. Park and C. J. Lee, *Chem. Phys. Lett.*, 2004, **383**, 104.
54 R. Liang, H. Cao, D. Qian, J. Zhang and M. Qu, *J. Mater. Chem.*, 2011, **21**, 17654.
55 S. Chen, J. Zhu, X. Wu, Q. Han and X. Wang, *ACS Nano*, 2010, **4**, 2822.
56 Y. Bai, M. Du, J. Chang, J. Sun and L. Gao, *J. Mater. Chem. A*, 2014, **2**, 3834.
57 B. P. Vinayan, R. Nagar, V. Raman, N. Rajalakshmi, K. S. Dhathathreyan and S. Ramaprabhu, *J. Mater. Chem.*, 2012, **22**, 9949.
58 M. L. D. Santos, R. C. Lima, C. S. Riccardi, R. L. Tranquilin, P. R. Bueno, J. A. Varela and E. Longo, *Mater. Lett.*, 2008, **62**, 4509
59 L. Ai and J. Jiang, *Chem. Eng. J.*, 2012, **192**, 156.
60 C. Hou, Q. Zhang, H. Wang and Y. Li, *J. Mater. Chem.*, 2011, **21**, 10512.
61 L. Jiang, M. Yao, B. Liu, Q. Li, R. Liu, H. Lv, S. Lu, C. Gong, B. Zou, T. Cui and B. Liu, *J. Phys. Chem. C*, 2012, **116**, 11741.
62 M. Srivastava, A. K. Das, P. Khanra, Md. E. Uddin, N. H. Kim and J. H. Lee, *J. Mater. Chem. A*, 2013, **1**, 9792.
63 D. Joung, V. Singh, S. Park, A. Schulte, S. Seal and S. I. Khondaker, *J. Phys. Chem. C*, 2011, **115**, 24494.
64 F. Gao, D. Zeng, Q. Huang, S. Tian and C. Xie, *Phys. Chem. Chem. Phys.*, 2102, **4**, 5651.
65 S. D. Perera, R. G. Mariano, K. Vu, N. Nour, O. Seitz, Y. Chabal, K. J. Balkus, Jr., *ACS Catal.* 2012, **2**, 949.
66 L. L. Zhang and X. S. Zhao, *Chem. Soc. Rev.*, 2009, **38**, 2520.
67 J. Zhang, J. Jiang, H. Li and X. S. Zhao, *Energy Environ. Sci.*, 2011, **4**, 4009.
68 L. S. Aravinda, K. U. Bhat and B. R. Bhat, *Mater. Lett.*, 2013, **112,** 158.

Table of Content

Dimensionally Integrated Nanoarchitectonics for Novel Composite from 0D, 1D, and 2D Nanomaterials: RGO/CNT/CeO_2 Ternary Nanocomposite with Electrochemical Performance

Raja Rajendran,[a,b] Lok Kumar Shrestha,*[a] Kosuke Minami[a], Munisamy Subramanian,[b] Ramasamy Jayavel,[b] and Katsuhiko Ariga[a]

Dimensionally mixed ternary nanocomposite from 2D graphene, 1D carbon nanotube, and 0D nanoparticles develops novel functions displaying enhanced electrochemical performance